

# Real-Time Voltage Stability Assessment for Load Areas Based on the Holomorphic Embedding Method

Chengxi Liu *Member, IEEE*, Bin Wang, *Student Member*, Fengkai Hu, *Student Member, IEEE*, Kai Sun, *Senior Member IEEE*, and Claus Leth Bak, *Senior Member IEEE*

**Abstract**—This paper proposes a method of real-time voltage stability assessment for load areas, in which the proximity to voltage collapse point at each bus can be accurately evaluated. Based on the non-iterative holomorphic embedding method (HEM), the voltage of each bus for different loading levels in the load area is quickly screened out by only performing one-time power flow calculation. A power series derived by the HEM with a physical germ solution makes sure that the P-V curve is in conformity with that from conventional continuous power flow. Therefore, the voltage stability margin can be evaluated by plugging a value into the embedded complex variable of the power series. An adaptive two-stage Pade approximants method is also proposed based on the power series to improve its convergence. Thus, on one hand, it enables more accurate prediction of the voltage collapse point; on the other hand, reduces the computational burden on large power systems. The proposed method is illustrated in detail on a 4-bus test system and then demonstrated on a load area of Northeast Power Coordinating Council 48-generators, 140-bus power system.

**Index Terms**—Continuous power flow, Holomorphic embedding method, Pade approximants, voltage stability assessment, voltage stability margin.

## I. INTRODUCTION

THE increase of electrical energy demand and the obstacle of concomitant infrastructure upgrading have driven electrical power systems operated closer to their stability limits. At present, electricity utilities are more concerned about the issues of voltage stability. A reliable, accurate, fast, on-line voltage stability assessment (VSA) is critical in the real-time operation environment for the utilities to not only identify areas vulnerable to voltage instability, especially under stressed system conditions, but also provide system operators with first-hand advice on control actions.

Many utilities have deployed synchronized phasor measurement units (PMUs) on transmission systems to provide real-time monitoring of voltage stability. These

measurement-based VSA approaches approximate the rest of the system by estimating parameters of Thevenin equivalent circuit. They rely on real-time synchronized data from PMUs placed on the boundary of load areas [1]–[4]. Thus, reduction of the load area to either an equivalent load bus or a simplified network is usually required because the full observability on every bus of the load area in real time is impractical. Furthermore, traditional state estimation based-VSA tools can not guarantee the convergence of the state estimator under stressed system conditions and thus would result in the decrease of accuracy for voltage instability prediction.

In this paper, a novel VSA approach based on power flow calculation using the holomorphic embedding method (HEM) is proposed to predict voltage instability at every bus of a load area. The proposed *physical germ solution* ensures that the embedded complex value is correspondingly equal to the overall loading level of all load buses. Therefore, fed by on-line measurements of active and reactive power of each load bus, the P-V curve for every bus can be accurately calculated by a one-time HEM calculation compared to traditional iterative continuous power flow (CPF). Besides, the adoption of adaptive Pade approximants based on the resultant power series of HEM can guarantee the convergence under stressed system conditions and accurately locate the voltage collapse point. This new VSA approach is promising to predict the voltage instability due to saddle-node bifurcation and provide the system operators with suggestions on control actions.

Traditionally, to solve the power flow equations (PFEs), many iterative numerical methods have been developed and adopted by commercialized power system software, including the Gauss-Seidel method, Newton-Raphson method and fast decoupled method. One major concern with these methods is that numerical divergence of iterations does not necessarily mean the non-existence of a power flow solution. As shown in [5], given an initial guess of the solution, the attraction region for, e.g., Newton-Raphson method, is fractal, not continuous, so that the convergence to the correct solution largely depends on the quality of the initial guess.

As a promising non-iterative method for solving PFEs on large systems, HEM was first proposed by A. Trias in [6]–[8]. The basic idea is to design a holomorphic function and to adopt its analytic continuation in the complex plane to find the solution of the PFEs as a power series about the embedded complex variable. That power series can be derived in a

---

This work was supported in part by NSF CURENT Engineering Research Center and NSF grant ECCS-1610025.

C. Liu, B. Wang and K. Sun are with Department of EECS, University of Tennessee, Knoxville, TN, USA (email: [cliu48@utk.edu](mailto:cliu48@utk.edu), [kaisun@utk.edu](mailto:kaisun@utk.edu), [bwang@utk.edu](mailto:bwang@utk.edu))

F. Hu is with Siemens Industry, Inc., Minneapolis, MN, USA (email: [fengkai.hu@siemens.com](mailto:fengkai.hu@siemens.com))

C. L. Bak is with Department of Energy, Aalborg University, Aalborg, Denmark (email: [clb@et.aau.dk](mailto:clb@et.aau.dk))

recursive manner, free from any guess of an initial solution. The original implementation demonstrates the HEM on systems with pure PQ buses plus a slack bus [6], and then on the systems with PV buses as well [9]-[15]. To enhance the convergence of the derived power series, references [6]-[15] suggest the use of Pade approximants or continued fractions, which, however, are not optimized. More efforts considering other load models are made by [14] for exponential loads and by [19] for nonlinear loads characterized by certain  $I$ - $V$  curves. The HEM is also extended to AC/DC power systems by [19]. Reported applications of the HEM and its variations include finding the low-voltage power flow solutions or unstable equilibrium points [20]-[21], network reduction [22], analyses of saddle-node bifurcation [16] and limit-induced bifurcation [23]. Although the superiority of the HEM can be seen by the existing literature, the precision issue could have a non-ignorable impact on the performance of the HEM, especially for heavily loaded and large systems [17], [21], [24].

In this paper, the proposed VSA approach based on the HEM can estimate the voltage stability margin (VSM) at each bus of a load area and predict the voltage instability as fast as real time. Superior to other power-flow methods, the HEM gives the whole P-V curve connecting the current operating point to the voltage collapse point for an anticipated scenario of load ramping. Thus, the VSM is directly obtained for each bus. Supplemented with load forecasting, this approach can predict the trend of voltage for early warning of voltage instability to system operators. The fast computation performance of HEM ensures the operators with enough time to take the necessary remedial actions.

The rest of this paper is organized as follows. Section II introduces the traditional HEM algorithm. Section III proposes a derivative embedding method starting from the physical germ solution on P-V curves. Section IV introduces the new VSA approach in detail, including the parameter identification of the external grid, online VSA scheme and adaptive Pade approximants method. Section V uses a 4-bus system to illustrate the advantages of this new method. Section VI tests the scheme on a load area of the Northeast Power Coordinating Council (NPCC) power system. Finally, conclusions are drawn in Section VII.

## II. CONVENTIONAL HOLOMORPHIC EMBEDDING LOAD FLOW METHOD

In mathematics, considering a complex-valued function  $x(s)$  of complex variable  $s = p + iq$ , with real part  $p$  and imaginary part  $q$ , if the embedded complex-valued function  $x(p+iq)$  satisfies Cauchy-Riemann equation in (1),  $x(s)$  is complex differentiable and thus holomorphic in a neighborhood of  $s$ -plane [25].

$$i \frac{\partial x}{\partial p} = \frac{\partial x}{\partial q} \quad (1)$$

Under this circumstance,  $x(s)$  can be represented in the form of a power series as (2) within its convergence region  $\mathcal{C}$ .

$$x(s) = \sum_{n=0}^{\infty} x[n]s^n, s \in \mathcal{C} \quad (2)$$

Thus, to solve a nonlinear equation of  $g(x)=0$ , a complex variable  $s$  is embedded into it to become a composition of  $s$ -function (3):

$$g(x) = g[x(s)] = 0. \quad (3)$$

The concept of HEM is to embed PFEs into a complex domain of  $s$ -plane, in which the analytic solution is originated from a common germ solution to contain the objective final solution. Therefore, this issue becomes how to design an  $x(s)$ , satisfying the following four criteria:

- 1) A common *germ* solution at  $s=0$  can be found for the equation  $g[x(s)]=0$ . For power flow calculation, the germ solution is normally designated as the solution under a no-load, no-generation condition.
- 2) Ensuring that  $g[x(s)]=0$  also holds true at  $s=1$  and the power series of  $\{x[n]s^n\}$  can be mathematically induced within a defined number of order  $N$ , through expanding and equating the coefficients of the same order  $s^n$  in  $g[x(s)]=0$ . Thus, the final solution of objective  $x$  is easily obtained by letting  $s=1$  in  $\sum x[n]s^n$ .
- 3) The embedded complex function  $g[x(s)]$  is required to be analytic continuous (holomorphic) along the path from germ solution at  $s=0$  to the final solution at  $s=1$ .
- 4) There is no exceptional point (branch point) along the path in  $s$ , where multiple solutions of  $g[x(s)]=0$  coalesce with each other. For PFEs, these exceptional points only coincide at the saddle-node bifurcation point.

Consider an  $N$  bus system composed of PQ buses, PV buses and slack buses, which are denoted as sets of  $\mathcal{P}$ ,  $\mathcal{V}$  and  $\mathcal{S}$  respectively. The original PFEs for PQ buses, PV buses and slack buses are expressed in the following (4)-(6), respectively.

$$\sum_{k=1}^N Y_{ik} V_i = \frac{S_i^*}{V_i}, \forall i \in \mathcal{P} \quad (4)$$

$$\begin{cases} P_i = \text{Re} \left( V_i \sum_{k=1}^N Y_{ik} V_k^* \right), \forall i \in \mathcal{V} \\ |V_i| = |V_i^{sp}| \end{cases} \quad (5)$$

$$V_i = V_i^{SL}, \forall i \in \mathcal{S} \quad (6)$$

where  $P_i$ ,  $Q_i$  and  $|V_i|$ ,  $\theta_i$  are the active power injection, reactive power injection and voltage magnitude, phase angle at bus  $i$ .  $V_k$  is bus voltage of bus  $k$  adjacent to bus  $i$ ,  $Y_{ik}$  is the admittance between bus  $i$  and bus  $k$ .

By the HEM formulation, the voltage of each bus and the reactive power of each PV bus are represented as power series functions of an embedded complex variable  $s$ , respectively, i.e.  $V(s)$  and  $Q(s)$ . Then, the  $s$ -embedded equations of PQ buses, PV buses and SL buses in (4)-(6) can be expressed as in (7)-(9) respectively. Note that, in order to maintain the holomorphy of the  $V(s)$ , its conjugate  $V^*$  should be defined by a separated function as  $V^*(s^*)$ , but not  $V^*(s)$ , more details can be found in [11].

$$\sum_{k=1}^N Y_{ik,trans} V_k(s) = \frac{s S_i^*}{V_i^*(s^*)} - s Y_{i,shunt} V_i(s), \forall i \in \mathcal{P} \quad (7)$$

$$\begin{cases} \sum_{k=1}^N Y_{ik,trans} V_k(s) = \frac{s P_i - j Q_i(s)}{V_i^*(s^*)} - s Y_{i,shunt} V_i(s) \\ V_i(s) V_i^*(s^*) = 1 + \left( |V_i^{sp}|^2 - 1 \right) s \end{cases}, \forall i \in \mathcal{V} \quad (8)$$

$$V_i(s) = V_i^{SL}, \forall i \in \mathcal{S} \quad (9)$$

### III. NEW HOLOMORPHIC EMBEDDING METHOD WITH PHYSICAL GERM SOLUTION

The conventional method separates the admittance matrix  $Y_{ik}$  into series part  $Y_{ik,trans}$  and shunt part  $Y_{ik,shunt}$  to ensure that the common germ solution has voltage equal to  $1\angle 0^\circ$  under the no-load no-generation condition at every bus in the network. Different from the conventional virtual germ solution, a physical germ solution is proposed in this paper with the no-load no-generation assumption only for PQ buses, while non-zero active power is specified and reactive power is injected into PV buses to adjust their voltage specifically to  $V_i^{sp}$ . There are three advantages of this new embedding approach. First, this proposed physical germ solution is on actual P-V curves that consider the power generation and voltage control at PV buses and no-load at PQ buses. Second, the embedded variable  $s$  can always be ensured to be the loading scale only controlling the loading level of the load buses (i.e. PQ buses), during which the active power generation of all PV buses is maintained as a constant or is controlled along the path of P-V curve on the  $s$ -plane. Third, in accordance with CPF in [26], this HEM with a physical germ solution can also enable integration of frequency control by specifying regulation factors of generators. The original PFE is recovered at  $s = 1$ . More importantly, the embedded complex-valued  $s$ -function is always endowed with physical meaning along the whole  $s$ -path from  $s = 1$  to collapse point: the reactive power injection of each PV bus is always adjusted to compensate the reactive power increase at PQ buses, until meeting its reactive power limit.

TABLE I. Physical germ solution of PFE for different bus types with HEM

Type	1 <sup>st</sup> Step ( $n = 0$ )	2 <sup>nd</sup> Step ( $n \geq 1$ )
PQ	$\sum_{k=1}^N Y_{ik} V_{gi}(s) = 0$	$\sum_{k=1}^N Y_{ik} V_{gi}(s) = 0$
PV	$\sum_{k=1}^N Y_{ik} V_{gi}(s) = 0$	$\sum_{k=1}^N Y_{ik} V_{gi}(s) = \frac{P_{gi}^* - jQ_{gi}(s)}{V_{gi}^*(s^*)}$ $V_{gi}(s)V_{gi}^*(s) =  V_{gi}^{sp} ^2$
SL	$V_{gi}(s) = V_i^{SL}$	$V_{gi}(s) = 0$

The procedure of finding this physical germ solution consists of two steps, shown in TABLE I. The first step is to find the initial condition under which the slack bus propagates its voltage to every bus of the network, while PV and PQ buses have zero injection to the grid, i.e.  $Q_g[0]=0$ , and (10)-(12).

$$\sum_{k=1}^N Y_{ik} V_{gi}[0] = 0, \forall i \in \mathcal{P} \quad (10)$$

$$\sum_{k=1}^N Y_{ik} V_{gi}[0] = 0, \forall i \in \mathcal{V} \quad (11)$$

$$V_{gi}[0] = V_i^{SL}, \forall i \in \mathcal{S} \quad (12)$$

Then the second step is to gradually adjust the reactive powers of PV buses to control their voltage magnitudes to the

specified voltage  $|V_i^{sp}|$  by recursively embedding a series of reactive power equal to  $Q_{gi}(s)$ . Meanwhile, the active power of each PV bus is fixed at the base value of the original condition.

Define  $W_{gi}(s)$  as a new inverse power series of  $V_{gi}^*(s^*)$ .

$$W_{gi}(s) = \frac{1}{V_{gi}^*(s^*)} = W_{gi}[0] + W_{gi}[1]s + W_{gi}[2]s^2 + \dots \quad (13)$$

If the initial voltage of germ solution  $V_{gi}[0]$  is calculated by (10)-(12), the term  $n$  of  $W_{gi}(s)$  and  $V_{gi}^*(s^*)$  can be calculated by convolution of terms 1 to  $n-1$  of  $V_{gi}^*(s^*)$  and  $W_{gi}(s)$  following (14) and (15). The subscript  $gi$  denotes the germ voltage of bus  $i$ .

$$W_{gi}[0] = \frac{1}{V_{gi}^*[0]} \quad (14)$$

$$W_{gi}[n]V_{gi}^*[0] + W_{gi}[0]V_{gi}^*[n] = -\sum_{m=1}^{n-1} W_{gi}[m]V_{gi}^*[n-m], n \geq 1 \quad (15)$$

Substitute  $W_{gi}(s)$  in (13) to the embedded PFE in 2<sup>nd</sup> column of TABLE I and expand them as (16) and (17) for PQ buses and PV buses respectively.

$$\sum_{k=1}^N Y_{ik} (V_{gi}[0] + V_{gi}[1]s + V_{gi}[2]s^2 + \dots) = 0, \forall i \in \mathcal{P} \quad (16)$$

$$\begin{cases} \sum_{k=1}^N Y_{ik} (V_{gi}[0] + V_{gi}[1]s + V_{gi}[2]s^2 + \dots) = [P_{gi} - j(Q_{gi}[0] + Q_{gi}[1]s + \dots)](W_{gi}[0] + W_{gi}[1]s + \dots) \\ (V_{gi}[0] + V_{gi}[1]s + V_{gi}[2]s^2 + \dots)(V_{gi}^*[0] + V_{gi}^*[1]s + V_{gi}^*[2]s^2 + \dots) = |V_{gi}^{sp}|^2 \end{cases} \quad (17)$$

Equating the coefficients of  $s, s^2 \dots$  up to  $s^n$  on both sides of (16) and (17), the terms  $V_{gi}[n]$  and  $Q_{gi}[n]$  are obtained by terms 0 to  $n-1$  of  $W(s)$  and  $Q(s)$ , based on (18) and (19).

$$\sum_{k=1}^N Y_{ik} V_{gi}[n] = 0, \forall i \in \mathcal{P} \quad (18)$$

$$\begin{cases} \sum_{k=1}^N Y_{ik} V_{gi}[n] = P_{gi}^* W_{gi}^*[n] - jQ_{gi}[n] W_{gi}^*[0] - j \left( \sum_{m=1}^{n-1} Q_{gi}[m] W_{gi}^*[n-m] \right), \forall i \in \mathcal{V} \\ V_{gi}[n] V_{gi}^*[0] + V_{gi}[0] V_{gi}^*[n] = \varepsilon[n-1] \end{cases} \quad (19)$$

where  $\varepsilon[n-1]$ , defined by (20) indicates the error of the voltage magnitude at PV buses, which will quickly converge to 0 just in several recursions by containing high order term  $V_{gi}[n]s^n$ .

$$\varepsilon[n-1] = \delta_{n1} \cdot \frac{1}{2} (|V_i^{sp}|^2 - |V_{gi}[0]|^2) - \frac{1}{2} \left( \sum_{m=1}^{n-1} V_{gi}[m] V_{gi}^*[n-m] \right) \quad (20)$$

$\delta_{ni}$  in (21) denotes coefficients that occur only for order of  $i = n$  and vanish for the other orders.

$$\delta_{ni} = \begin{cases} 1 & \text{if } n=i \\ 0 & \text{otherwise} \end{cases} \quad (21)$$

TABLE II. Final solution of PFE for different bus types with HEM

Type	Physical germ solution ( $n = 0$ )	Final solution ( $n \geq 1$ )
PQ	$\sum_{k=1}^N Y_{ik} V_i(s) = 0$	$\sum_{k=1}^N Y_{ik} V_i(s) = \frac{s(P_{gi} - jQ_{gi})}{V_i^*(s^*)}$
PV	$\sum_{k=1}^N Y_{ik} V_i(s) = S_{ig}^*$ $V_i(s)V_i^*(s) =  V_i^{sp} ^2$	$\sum_{k=1}^N Y_{ik} V_i(s) = \frac{S_{ig}^* - jQ_{gi}(s)}{V_i^*(s^*)}$ $V_i(s)V_i^*(s) =  V_i^{sp} ^2$
SL	$V_i(s) = V_i^{SL}$	$V_i(s) = 0$

In (19),  $V_{gi}[n]$  and  $W_{gi}[n]$  are unknown complex numbers, and  $Q_{gi}[n]$  is an unknown real number. Moving all unknowns

of the  $n$ th order to the left hand side and breaking the PFE into real and imaginary parts, a matrix equation is created containing all  $V_{gi}[n]$ ,  $W_{gi}[n]$  and  $Q_{gi}[n]$ . There are 5 real unknowns in total for each PV bus, as  $V_{gi}[n]$  and  $W_{gi}[n]$  are complex valued, while  $Q_{gi}[n]$  is a real number. Assume that there are  $l$  slack buses,  $m$  PQ buses and  $p$  PV buses in the  $N$ -bus network. Then, the dimension of the matrix equation equals to  $2l+2m+5p$ .

After finding the physical germ solution, the rest of the process is similar to the conventional HEM. Table II shows the solutions of PFEs for PQ, PV and SL buses with physical load embedding, where  $s$  represents the loading level only for PQ buses. The difference mainly lies on the right hand side that  $s$  is multiplied by the complex load of the PQ bus, so the voltage of PQ bus only depends on the previous step  $W[n-1]$ . Note that, different from the conventional HEM during the process of embedding, the active powers of PV buses are not multiplied by  $s$ , indicating invariant generation outputs under load increase. However, if frequency control of PV buses is taken into account for dynamic load flow, an additional term with generation regulation factor  $\alpha_i$  is attached in (22) to represent the effect of frequency control, in which  $\alpha_i P_{gi}$  represents the increase rate of active power of generator  $i$  with respect to the overall load variation.

$$\sum_{k=1}^N Y_{ik} V_i(s) = \frac{(P_{gi} - jQ_{gi}) + s(\alpha_i P_{gi}) - jQ_i(s)}{V_i^*(s^*)}, \forall i \in \mathcal{V} \quad (22)$$

#### IV. REAL TIME VOLTAGE STABILITY ASSESSMENT

##### A. Identification of External System Parameters

For a load center fed by external generation through multiple tie lines, those tie lines may have different power transfer limits in terms of voltage stability, especially in the case that their coupling is weak. Like the  $N+1$  buses equivalent system, proposed in [4], the external system by a single voltage source  $E$  connected to  $N$  boundary buses of the load area respectively by  $N$  branches with impedances  $z_{E1} \sim z_{EN}$ , as shown in Fig. 1. Thus the coupling relationship among tie lines and boundary buses are retained. Unlike that  $N+1$  buses equivalent, all buses in the load area are retained in this paper and their VSMs will be calculated by the proposed HEM.

Sequential Quadratic Programming (SQP) method is applied to identify the parameters of external grid, i.e.  $E$  and  $z_{E1} \sim z_{EN}$ , using synchronized data of complex power  $S_i$  and voltage phasor  $V_i$  measured at the boundary buses [27].

Assuming  $K$  measurement points in a time window were obtained by PMUs,  $V_i(k) = |V_i(k)| \angle \theta_i(k)$  and  $S_i(k) = P_i(k) + jQ_i(k)$  are defined respectively as the received complex power and voltage phasor at boundary bus  $i$  at time point  $k$ . Therefore, the parameters of the external system can be obtained by solving the following optimization problem,

$$\min J^{\text{ex}} = \sum_{k=1}^K \sum_{i=1}^N \frac{\omega_e}{N} [e_i^{\text{ex}}(k)]^2 + \sum_{i=1}^N \omega_r \left( \frac{r_{Ei}}{r_{EP}} - 1 \right)^2 + \sum_{i=1}^N \omega_z \left( \frac{x_{Ei}}{x_{EP}} - 1 \right)^2 \quad (23)$$

s.t.  $E > 1, r_{Ei} \geq 0$

where the 1<sup>st</sup> term gives the estimation errors for power flow equations for all time instants. The error at time instant  $k$  is

defined as (24)

$$e_i^{\text{ex}}(k) = E - \left| (P_i(k) - jQ_i(k))(r_{Ei} + jx_{Ei}) + (V_i(k))^2 \right| / V_i(k) \quad (24)$$

The 2<sup>nd</sup> and 3<sup>rd</sup> terms summate normalized differences in resistance  $r_{Ei}$  and reactance  $x_{Ei}$  of  $z_{Ei}$  between the estimates for the current and previous time windows.  $\omega_e$  and  $\omega_z$  are the weighting factors respectively for variances of  $E$  and  $z_{Ei}$  over the time window.

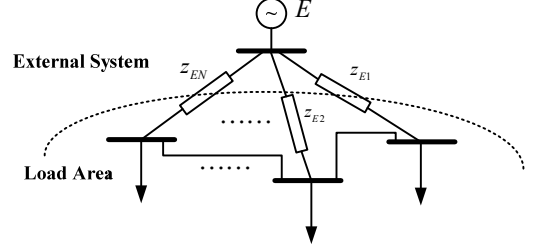


Fig. 1. Reduction of the external area to a voltage source.

As the equivalent parameters of the external system are updated in real time by solving the above optimization problem, the HEM-based online VSA scheme can be performed directly on the reduced system in Fig. 1.

##### B. Online Voltage Stability Assessment

The principle of this HEM-based online VSA scheme is illustrated in Fig. 2. The  $x$ -axis and  $y$ -axis represent the active and reactive power of bus  $i$ . The voltage stability boundary represents the voltage collapse point with respect to different power factor angles  $\phi$ . The point  $OC_0$  is the original operating condition, where  $s_0 = 1$ . After the implementation of this proposed HEM, the P-V curve can be obtained by plugging in  $s$  into the power series of  $V(s)$  under the assumption that all loads are scaled up simultaneously at the same rate and the power factor of each load is maintained invariant.

Then adaptive Pade approximants help to accurately predict the voltage collapse point  $sc_t$ , which will be introduced in the next sub-section. The VSM of overall system is defined in (25), where  $sc_t$  represents the maximum loading scale until voltage collapse at time  $t$ . VSM physically means the maximum limit of the loading scale to maintain the voltage stability of the load area.

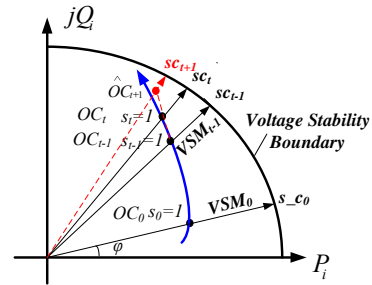


Fig. 2. Illustration of HEM-based VSA.

It can be assumed that the active power, reactive power and voltage of every bus of the load area are obtained from the real-time state estimator, e.g., every 30 seconds [28]. Practically, the loads may vary randomly in a load area. A prediction of load for the next 30 seconds is adopted. As shown in the red dot in Fig. 2, the predicted OC at time  $t+1$  is

based on the linear extrapolation of previous steps, as defined in (26).  $S_{i,t}$  denotes the complex power of node  $i$  at time  $t$ . The calculation of HEM is always finished within 2 second, which can definitely guarantee enough time for VSM estimation for the next 30 seconds.

$$VSM_i = sc_i - 1 \quad (25)$$

$$S_{i,t+1} = S_{i,t} + \Delta S_{i,t} = 2S_{i,t} - S_{i,t-1} \quad (26)$$

### C. Adaptive Two-stage Pade approximation

As mentioned in previous section, voltage can be expressed in the form of power series (27) by the HEM. However, precision issue could have a non-ignorable impact on the performance of the HEM, especially for heavily stressed conditions of large power systems. The reason of this problem lies on the limited convergence region of the Taylor series. Practically, double precision calculation with 16-digits easily becomes exhausted to decrease the errors of PFEs to less than  $1e-13$ . An alternative solution is to increase the arithmetic precision to much higher digits, i.e. 2000 digits, but the convergence region still can not be extended to the edge of stability boundary [24]. From Stahl's Pade convergence theory in [29] and [30], the diagonal or close to diagonal Pade approximants converges to the original function in maximum domain, if the original function is holomorphic. In other words, Pade approximants have the best convergence performance with equal or nearly equal orders between the numerator and denominator, i.e.  $|L-M| \leq 1$  in (28). Different from the conventional HEM using Pade approximants to determine the convergence of load flow [6]-[8], an adaptive two-stage algorithm is proposed here to find the optimal order of Pade approximants for each voltage. Viskovatov's method is adopted here to find the coefficients of Pade approximants [31]. This is carried out as a post-process after the HEM with normal double precision arithmetic computation.

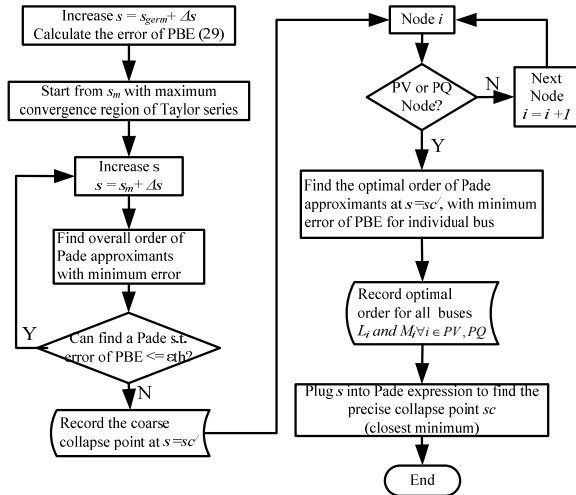


Fig. 3. Flowchart of adaptive two-stage Pade approximants to find the collapse point of the power system.

$$V_i(s) = \sum_{n=0}^N V_i[n]s^n \quad (27)$$

$$V_i(s) = \sum_{l=0}^L a_l s^l / \sum_{m=0}^M b_m s^m = \frac{a_0 + a_1 s + a_2 s^2 + \dots + a_L s^L}{b_0 + b_1 s + b_2 s^2 + \dots + a_M s^M} \quad (28)$$

As shown by the flowchart in Fig. 3, the adaptive Pade approximants method consists of two stages of finding the coarse collapse point at  $sc$  and precise collapse point at  $sc'$ . The first stage is to plug values of  $s$  into the Taylor series of PQ and PV nodes created by the HEM to find the maximum convergence region of Taylor series at  $s = s_m$ , shown as point A in Fig. 4. Then starting from point A at  $s = s_m$ , the overall best order of Pade approximants for all buses is found to make the errors of PFEs be a minimum value  $\varepsilon(s)$ . The following process is to increase  $s$  until the coarse collapse point at  $s = sc$  is found where the overall minimum  $\varepsilon(s)$  can no longer be less than a preset threshold  $\varepsilon_{th}$ , shown as point B in Fig. 4. This process is defined by equation in (29). The second stage is to find the optimal order of Pade approximants for individual bus  $i$  at  $s = sc'$ . The optimal order for individual bus  $i$  is recorded as  $L_i$  and  $M_i$ , so the Pade expression of voltage is obtained by truncating  $[L_i/M_i]$  orders in (28). Finally, the precise collapse point is found by searching the local minima of all buses at  $sc_i$  and selecting the minimum  $sc_i$  of all buses as the final precise collapse point at  $sc$  (30), shown as point C in Fig. 4.

$$sc' = \max s, \text{ s.t.}$$

$$\varepsilon(s) = \min_N \left[ \sum_{j=1}^N Y_{ij} V_i(s) - \frac{s S_i^*}{V_i^*(s^*)} \right]_{i=1} \leq \varepsilon_{th}, \forall i \in \mathcal{P} \cup \mathcal{V} \quad (29)$$

$$sc = \min_i sc_i = \min_i \left( \min_{M_i, L_i} \varepsilon(sc') \right), \forall i \in \mathcal{P} \cup \mathcal{V} \quad (30)$$

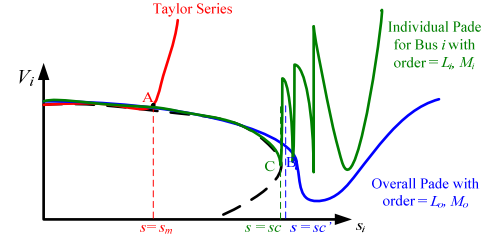


Fig. 4. Illustration of adaptive two-stage Pade approximants.

## V. DEMONSTRATION ON A 4-BUS POWER SYSTEM

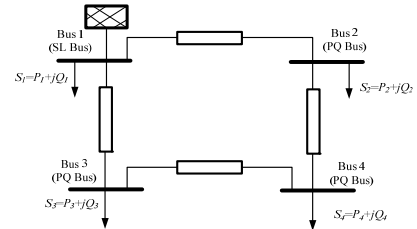


Fig. 5. One-line diagram of the 4-bus power system

As shown in Fig. 5, a 4-bus system modified from that in [32] is first used to illustrate the proposed VSA approach. It has a voltage source supporting three constant power loads. The system is simulated in the software DlgSILENT/PowerFactory with gradual load increase from the original operating condition. Two cases are simulated considering two types of load profiles.



### A. Case A: Loads increasing at the same rate

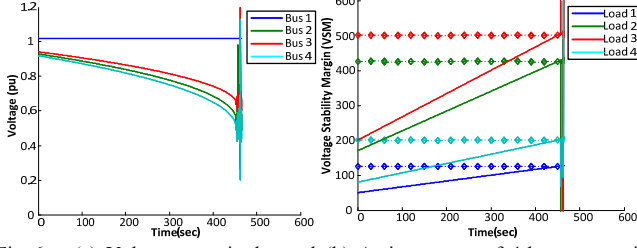


Fig. 6. (a) Voltage magnitudes and (b) Active power of 4-bus system in Case A.

The power consumption of all loads are gradually ramped up from the original load at the same rate and their power factors are kept unchanged. It can be identified by the voltage magnitudes in Fig. 6(a) that voltage collapse happens at  $t=456s$ , which is accurately predicted by the results from the HEM as shown in Fig. 6(b), where active powers at all buses cross their respective voltage stability limits at the same time. The diamond markers connected to a horizontal dash-dot lines in Fig. 6(b) indicate the voltage limit of each bus calculated by the HEM and updated every 30 seconds. This case has invariant voltage stability limits for all buses, because an ideal voltage source is connected and all loads increase in the same pattern.

### B. Case B: Loads increasing at different random rates with variable power factors

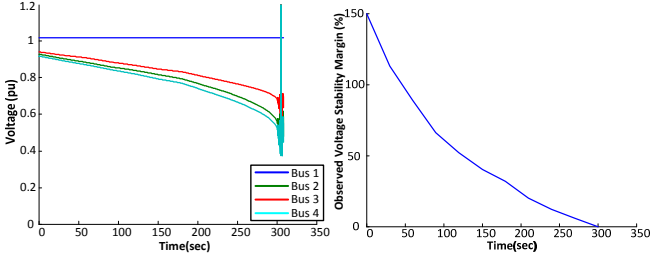


Fig. 7. (a) Voltage magnitudes and (b) VSM of 4-bus system in Case B.

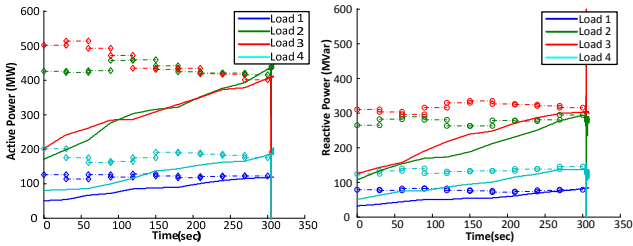


Fig. 8. Power and stability boundary of 4-bus system in Case B (a) active power (b) reactive power.

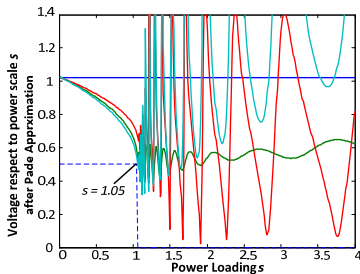


Fig. 9. The voltage w. r. t. power scale predicted by HEM at  $t=240s$ .

The active power and reactive power of all loads are gradually increased at random rates, ranging between 0% and 30% of their original loading every 30 seconds. Seen from voltage magnitudes of the 4-bus system in Fig. 7(a), voltage collapse happens at  $t = 301s$ . This voltage collapse is accurately predicted by the VSM from the HEM in Fig. 7(b). Fig 8 compares the active and reactive powers of each load to the voltage stability limits, which are shown by the dash-dot lines and updated every 30 seconds based on the result of state estimation and load pattern forecast. Also, note that, in Fig. 8(a), the active powers of Loads at buses 2, 3 and 4 cross their limits at different times, i.e.  $t = 289s$ ,  $295s$  and  $289s$ , respectively. Thus, voltage instability may originate from buses 2 and 4, where remedial actions should be taken firstly.

Fig.9 shows the voltage with respect to the overall power scale predicted by the HEM at  $t = 240s$ . This collapse power scale is 1.05, so the VSM is only 5%, which means that if the loads in the next 30sec ramp up at an unchanged rate, the power can only increase by 5% at the end of the next period, i.e. at  $t = 270sec$ , with only 5% margin left.

## VI. CASE STUDY ON THE NPCC TEST SYSTEM

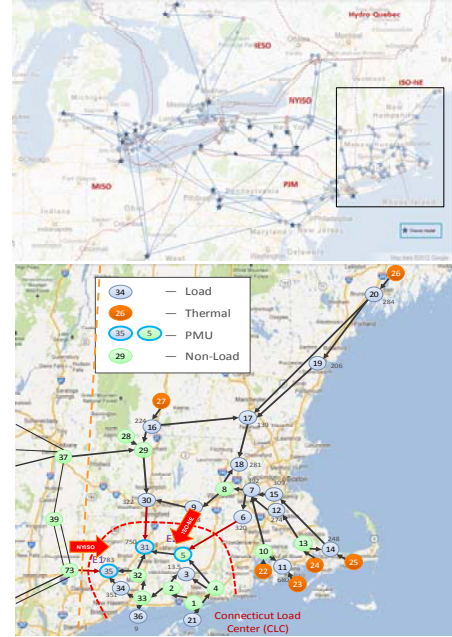


Fig. 10. Map of NPCC system and CLC load area (a) system topology (b) CLC area.

The NPCC system with 48 generators and 140 buses in [33] is adopted to demonstrate the proposed HEM-based VSA method. As shown in Fig. 10, the Connecticut Load Center (CLC) area is supported by three tie lines, i.e. 73-35, 30-31 and 6-5. Assume that all 3 tie lines are equipped with PMUs at boundary buses 35, 31 and 5 of the load area. PowerFactory is used to simulate the voltage instability scenarios in the following cases. The load at each bus of the area is modeled as constant power load. If the load has a constant impedance component, that will be integrated into the admittance matrix  $Y_{ik}$ . For more general load models, reference [14] describes a method to integrate the more general ZIP load model or

exponential load model into the HEM. All buses in load area are measured by SCADA system and the state estimation results on the load area are updated every 30s. Thus, the HEM-based VSA scheme aims at predicting voltage instability in the next 30s period. If real-time synchronized phasor data are available at all buses by either PMUs or a faster state estimator, the proposed scheme may provide real-time VSM at each bus.

#### A. Case A: Load increasing at same rate

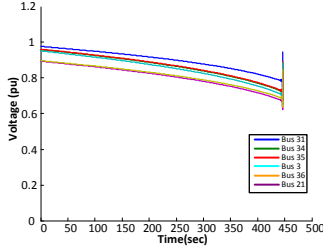


Fig. 11. Voltage magnitudes with Case A.

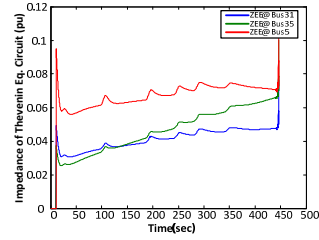


Fig. 12. Real-time estimation of the impedance of equivalent branches.

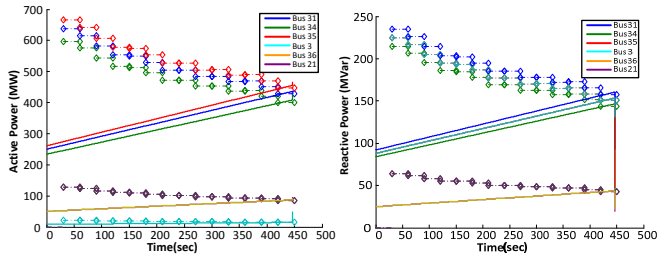


Fig. 13. Active and reactive powers and stability limits with Case A  
(a) active power (b) reactive power.

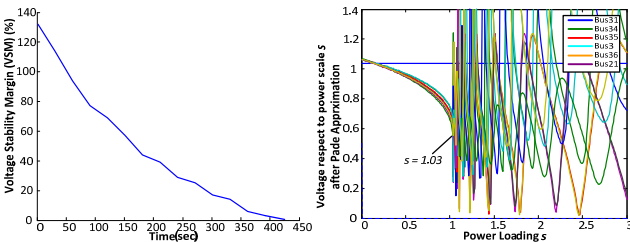


Fig. 14. (a) VSM and (b) the voltage w. r. t. power scale predicted by the HEM at  $t=420$ s for Case A.

This case increases load at all buses of the area at a same rate of 0.16% per second. Fig. 11 shows that voltages gradually decrease and then collapse at  $t=456.3$ s. The external system is aggregated to an equivalent voltage source  $E$  radially connected to three boundary buses of the load area by three branches. Fig. 12 gives the estimates of the branch impedance to buses 31, 35 and 5. The voltage collapse is predicted by the active and reactive powers meeting their limits in  $t=420$ -450s,

as shown in dash-dot lines in Fig. 13. Compared to Case A of the 4-bus system, the variations in stability limits are caused by the changes in the external system and consequently in their equivalent parameters. As shown in Fig. 14(a), at  $t=420$ s the VSM decreases to 3%, which gives the last warning of voltage instability and indicates the last chance to take a remedial action, e.g. switching in a shunt capacitor in the load area. Fig. 14(b) gives the voltage with respect to power scale  $s$  predicted by the HEM at  $t=420$ s, and a precise collapse load scale  $s_c=1.03$ .

#### B. Case B: Loads increasing at different random rates with variable power factors

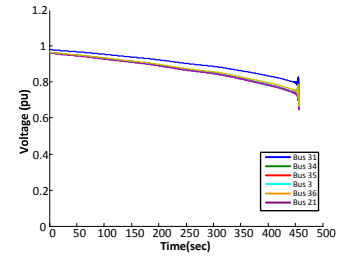


Fig. 15. Voltage magnitudes with Case B.

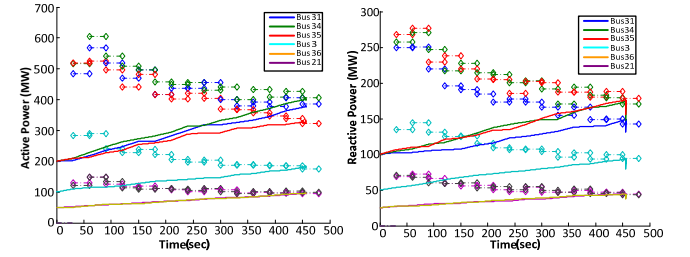


Fig. 16. Active and reactive powers and stability limits with Case B  
(a) active power (b) reactive power.

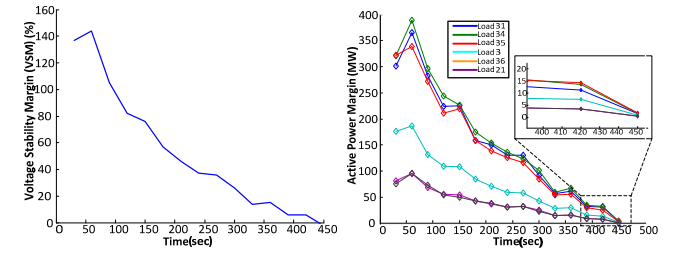


Fig. 17. (a) VSM and (b) Active power margin for each bus predicted by the HEM for Case B.

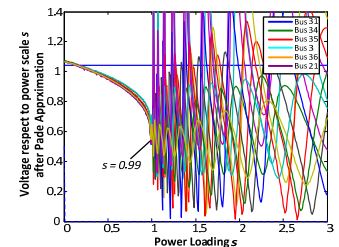


Fig. 18. Voltage w. r. t. power scale predicted by HEM at  $t=450$ s for Case B.

In this case, a more realistic scenario with loads increasing at a random rate in 0-10% per 30 second is tested. The voltage collapse happens at  $t=452$ s, as shown in Fig. 15. The last warning is armed between  $t=420$ s and  $t=450$ s, since loads at Bus 3, 34 and 21 cross their individual stability limits as

shown in Fig. 16 (a) and (b) for active power and reactive power respectively. The VSM at  $t = 450$ s from Fig. 17(a) is below 0, indicating the occurrence of voltage instability. Fig. 17(b) shows the margin for active power for each load bus predicted by the HEM, in which the margin of Bus 3, 34 and 21 are closer to their limits than other buses. Fig. 18 shows the voltage with respect to power scale  $s$  predicted by the HEM at  $t = 450$ s, in which the precise collapse load scale  $sc = 0.99$  signals the voltage collapse immediately after  $t = 450$ s.

The real-time HEM-based VSA scheme is able to provide system operators with a timely and accurate indication of the VSM. Practically, a more conservative threshold of VSMs should be pre-configured, e.g. 15%, on one hand to give operators enough time to activate emergency voltage control. On the other hand, it leaves enough stability margin to prevent the voltage collapse. All computations of this new scheme can be finished within 2 seconds in MATLAB, including external parameter identification, power flow prediction, the proposed HEM, and adaptive Pade approximants, so the overall VSM and individual VSM for each bus is given about 28 seconds before the real time. If each bus is equipped with a PMU to provide synchronized phasor data at a higher frequency, e.g. 30-60Hz, operators can monitor the load change and the VSM at each load bus with higher accuracy and to decide more precisely whether and when a remedial action is needed.

## VII. CONCLUSION

This paper proposed a new online VSA scheme for a load area based on the proposed HEM with a physical germ solution. The new method can quickly monitor the VSM of a load area, predict the voltage instability and suggest system operators the timing and location to take remedial actions. An adaptive two-stage Pade approximants method is also proposed to extend the convergence region of the Taylor series, making the algorithm applicable for large power systems. This new method has been demonstrated on the 140-bus NPCC system.

Compared with traditional simulation-based VSA method, the proposed scheme can guarantee its convergence and accuracy under stressed system conditions. Compared to other measurement-based approaches, this new scheme avoids network reduction on the load area. Also, this scheme integrates real-time load prediction at each bus to provide more credible margin information.

## REFERENCES

- [1] K. Vu *et al.*, "Use of local measurements to estimate voltage-stability margin," *IEEE Trans. Power Syst.*, vol. 14, no. 3, pp. 1029-1035, Aug. 1999.
- [2] B. Milosevic and M. Begovic, "Voltage-stability protection and control using a wide-area network of phasor measurements," *IEEE Trans. Power Syst.*, vol. 18, no. 1, pp. 121-127, Feb. 2003.
- [3] M. Glavic and T. Van Cutsem, "Wide-area detection of voltage instability from synchronized phasor measurements. Part I: Principle," *IEEE Trans. Power Syst.*, vol. 24, no. 3, pp. 1408-1416, Aug. 2009.
- [4] F. Hu, K. Sun *et al.*, "Measurement-based real-time voltage stability monitoring for load areas," *IEEE Trans. Power Systems*, vol. 31, no. 4, pp. 2787-2798, Jul. 2016.
- [5] J. Thorp, S. Naqavi, "Load flow fractals," *IEEE 28<sup>th</sup> Ann. Conf. Decis. Contr.*, Dec. 1989.
- [6] A. Trias, "The Holomorphic Embedding Load Flow Method," *IEEE PES GM*, San Diego, CA, Jul. 2012.
- [7] A. Trias, "System and method for monitoring and managing electrical power transmission and distribution networks," US Patents 7 519 506 and 7 979 239, 2009-2011.
- [8] A. Trias, "Fundamentals of the holomorphic embedding load-flow method" *arXiv:1509.02421v1*, Sep. 2015.
- [9] S. S. Baghsorkhi and S. P. Suetin, "Embedding AC Power Flow with Voltage Control in the Complex Plane: The Case of Analytic Continuation via Padé Approximants," *arXiv:1504.03249*, Mar. 2015.
- [10] M. K. Subramanian, Y. Feng and D. Tylavsky, "PV bus modeling in a holomorphically embedded power-flow formulation," *North American Power Symposium (NAPS)*, Manhattan, KS, 2013.
- [11] M. K. Subramanian, "Application of Holomorphic Embedding to the Power-Flow Problem," *Master Thesis*, Arizona State Univ., Aug. 2014.
- [12] A. Trias, "Fundamentals of the Holomorphic Embedding Load-Flow Method," *arXiv.org: 1509.02421*, Sep. 2015.
- [13] I. Wallace, D. Roberts, A. Grothey, K. I. M. McKinnon, "Alternative PV bus modelling with the holomorphic embedding load flow method," *arXiv:1607.00163*, Jul. 2016.
- [14] S. S. Baghsorkhi, S. P. Suetin, "Embedding AC power flow in the complex plane part I: modelling and mathematical foundation," *arXiv:1604.03425*, Jul. 2016.
- [15] S. Rao, Y. Feng, D. J. Tylavsky, M. K. Subramanian, "The holomorphic embedding method applied to the power-flow problem," *IEEE Trans. on Power Syst.*, vol. 31, no. 5, pp. 3816-3828, Sep. 2016.
- [16] S. Rao, D. J. Tylavsky, Y. Feng, "Estimating the saddle-node bifurcation point of static power systems using the holomorphic embedding method," *International Journal of Electrical Power and Energy Systems*, vol. 84, no. x, pp. 1-12, 2017.
- [17] Y. Li, "Effect of various holomorphic embeddings on convergence rate and condition number as applied to the power flow problem," *Master Thesis*, Arizona State Univ., Nov. 2015.
- [18] S. Chevalier, "Using real time statistical data to improve long term voltage stability in stochastic power systems," *Master Thesis*, Univ. of Vermont, Oct. 2016.
- [19] A. Trias, J. L. Marin, "The holomorphic embedding loadflow method for DC power systems and nonlinear DC circuits," *IEEE Trans. on Circuits and Systems-I: regular papers*, vol. 63, no.2, pp. 322-333, Sep. 2016.
- [20] Y. Feng and D. Tylavsky, "A novel method to converge to the unstable equilibrium point for a two-bus system," *North American Power Symposium (NAPS)*, Manhattan, KS, 2013.
- [21] Y. Feng, "Solving for the low-voltage-angle power-flow solutions by using the holomorphic embedding method," *Ph.D. Dissertation*, Arizona State Univ., Jul. 2015.
- [22] S. Rao and D. Tylavsky, "Nonlinear network reduction for distribution networks using the holomorphic embedding method," *North American Power Symposium (NAPS)*, Denver, CO, USA, 2016.
- [23] S. S. Baghsorkhi, S. P. Suetin, "Embedding AC power flow in the complex plane part II: a reliable framework for voltage collapse analysis," *arXiv:1609.01211*, Sep. 2016.
- [24] B. Schmidt, "Implementation and evaluation of the holomorphic embedding load flow method," *Master Thesis*, Technical Univ. Munchen, Mar. 2015.
- [25] M. R. Range, *Holomorphic Functions and Integral Representations in Several Complex Variables*, Springer-Verlag, New York, Inc. 2002.
- [26] V. Ajarapu and C. Christy, "The continuation power flow: a tool for steady state voltage stability analysis," *IEEE Trans. Power Syst.*, vol. 7, no. 1, pp. 416-423, Feb. 1992.
- [27] J. Nocedal and S. J. Wright, *Numerical Optimization*, 2<sup>nd</sup> ed. New York, NY, USA: Springer, 2006.
- [28] A. Abur and A. G. Exposito, *Power System State Estimation*, Marcel Dekker, New York, Inc. 2004.
- [29] H. Stahl, "On the convergence of generalized Pade approximants," *Constructive Approximation*, vol. 5, pp. 221-240, 1989.
- [30] H. Stahl, "The convergence of Pade approximants to functions with branch points," *Journal of Approximation Theory*, vol. 91, no. 2, pp. 139-204, 1997.
- [31] A. Cuyt *et al.*, *Handbook of Continued Fractions for Special Functions*, Springer, ISBN: 978-1-4020-6948-2.
- [32] J. Grainger, W. Stevenson, *Power System Analysis*, pp. 337-338, McGraw-Hill, 1994.
- [33] J. H. Chow *et al.*, "Inertial and slow coherency aggregation algorithms for power system dynamic model reduction," *IEEE Trans. Power Syst.*, vol. 10, no. 2, pp. 680-685, May 1995.